CARBON 51 (2013) 236–242

Available at www.sciencedirect.com

SciVerse ScienceDirect

journal homepage: www.elsevier.com/locate/carbon

Graphene-based transparent strain sensor

Sang-Hoon Bae [a], *Youngbin Lee* [a], *Bhupendra K. Sharma* [a], *Hak-Joo Lee* [b], *Jae-Hyun Kim* [b,*], *Jong-Hyun Ahn* [a,*]

[a] *School of Advanced Materials Science & Engineering and SKKU Advanced Institute of Nanotechnology (SAINT), Sungkyunkwan University, Suwon 440-746, South Korea*

[b] *Department of Nano Mechanics, Nano Convergence and Manufacturing Systems Research Division, Korea Institute of Machinery & Materials, 104 Sinseongno, Yuseong, Daejeon 305-343, South Korea*

ARTICLE INFO

Article history:
Received 15 June 2012
Accepted 17 August 2012
Available online 27 August 2012

ABSTRACT

Transparent strain sensors based on graphene were fabricated in a form of rosette on a flexible plastic or stretchable rubber substrate by using reactive ion etching and stamping techniques. Their piezoresistive properties were investigated under a tensile strain up to 7.1%. We demonstrated this sensor on a transparent glove and measured magnitudes and directions of the principal strains on the glove induced by the motion of fingers.

1. Introduction

Over the past decades, strain sensors have been of great interest among researchers. Strain sensors are required to detect deformations or structural change occurring in our surrounding infrastructures as well as the internal activities in human bodies. To fabricate an efficient strain sensor, researchers are in search of a material that can exhibit large structural change in response to a small applied strain [1–4].

Graphene is another class of carbon based material. It has a two-dimensional (2D) network of SP^2 hybridized carbon atoms packed into a hexagonal structure, and recently, it has become a potential candidate for strain sensor because of its good mechanical properties [5]. Enormous efforts have been devoted to exploration of its many applications in the field of science and engineering [6–10]. However, very few investigations have been carried out to explore the applications of graphene for testing the devices subjected to strain/stress and pressure effects even though it has various advantages over carbon nanotubes such as easy pattern formation, and optical transparency [11–20]. Lee et al. [11] reported the piezo-resistance response of graphene and the graphene based strain sensor with a gauge factor of 6.1. Fu et al. [12] also demonstrated a monolayer graphene based strain sensor with high sensitivity. Furthermore, Wang et al. [14] showed that graphene can be used under high strain over 30% using fully reversible structural geometry. Recently, the incorporation of flexibility and transparency with the devices has become a great challenge for researchers attempting to develop human-interface electronics [21]. In this context, the excellent stretchability and good transparency of graphene provide a way to realize a new class of human-interface devices for real-life applications. Therefore, a detailed investigation and experimental demonstration of graphene-based strain sensors are quite important for the exploration of future applications in human-interface technology.

In this article, we demonstrate a graphene-based strain sensor with the capability to monitor the motion of body parts. The strain sensor was fabricated on very thin, flexible plastic or stretchable rubber substrates, using a traditional micro-fabrication process. In general, a single strain gauge can measure strain in only one direction, which, as a result, is of limited practical use, unless the predominant strain direction is known and constant, and the gauges are aligned along it. In order to detect the changes in strain direction during various activities of the human body, we also demonstrated rosette gauges based on graphene installed on a hand glove, and simultaneously measured the magnitude and

* *Corresponding authors:* Fax: +82 42 868 7550 (J.-H. Kim), fax: +82 31 290 7400 (J.-H. Ahn).
E-mail addresses: jaehkim@kimm.re.kr (J.-H. Kim), ahnj@skku.edu (J.-H. Ahn).

0008-6223/$ - see front matter
http://dx.doi.org/10.1016/j.carbon.2012.08.048

direction of the principal strains during bending motion of a finger.

2. Experimental details

Fig. 1a shows the schematic representation of key fabrication steps for the flexible and transparent graphene-based strain sensors employed in this study. The 300 nm Ni catalyst layer was deposited on SiO_2/Si using electron-beam evaporator, where the SiO_2 was formed by dry oxidation method. Then, we used chemical vapor deposition (CVD) method to grow the graphene on Ni catalyst layers described elsewhere [22]. The conventional optical photolithography was used to pattern the graphene films and followed by the reactive ion etching (RIE) with a power of 100 W and O_2 etching gas of 20 SCCM to get graphene films of the desired shape and dimension. After that, we attached a polydimethylsiloxane (PDMS) film of 2 mm thickness to the patterned graphene on Ni/SiO_2/Si substrate. The patterned graphene was then transferred on the PDMS film by etching Ni/SiO_2 layer and subjected to a uniaxial tensile test. We also fabricated the two types of graphene strain sensors in a form of rosette by arranging three identical strain sensors in an equilateral triangle with 120° angles. The two types of graphene strain sensors were of identical shape and dimensions, but the thicknesses of their target PDMS substrates were different with each other since it was necessary to investigate the functionalities of the graphene strain sensors depending on the substrate thickness in the experimental demonstration. For one type of graphene strain sensor, we attached the thick PDMS film (2 mm) to the patterned graphene. For another we spin coated (4000 rpm, 50 s) a PDMS solution over a Si wafer and heated the PDMS/Si up to 70 °C to cure it. After that, it was attached to the rosette graphene sensor on Ni/SiO_2/Si substrate. The thickness of the spin-coated PDMS thin film was measured to be 500 μm. Other processing steps, such as detaching the Si substrate and washing, followed the same methods and sequences as those for single strain sensors. Fig. 1b shows a photograph of the proposed graphene-based strain sensor. This strain sensor can be attached to any target substrate using epoxy. To demonstrate the glove equipped with strain sensor, we attached it to the glove using epoxy. In this experiment, the rosette gauge of graphene fabricated on a thinner PDMS substrate was transferred to a wearable hand glove for experimental demonstration of the detection of strain induced by motion of a finger while the other rosette gauge strain sensor fabricated on the thick PDMS was subjected to a stretching measurement using a motorized tensile machine.

To measure the electrical properties of the strain sensor, the graphene based strain sensors were first put on the step motor to apply strain to the sensors. The strain sensors were stretched and simultaneously measured using a source-meter. Gold wire was used to connect the strain sensor to a terminal. Lab-view software was used to control the process of data acquisition from strain sensors, and the complete

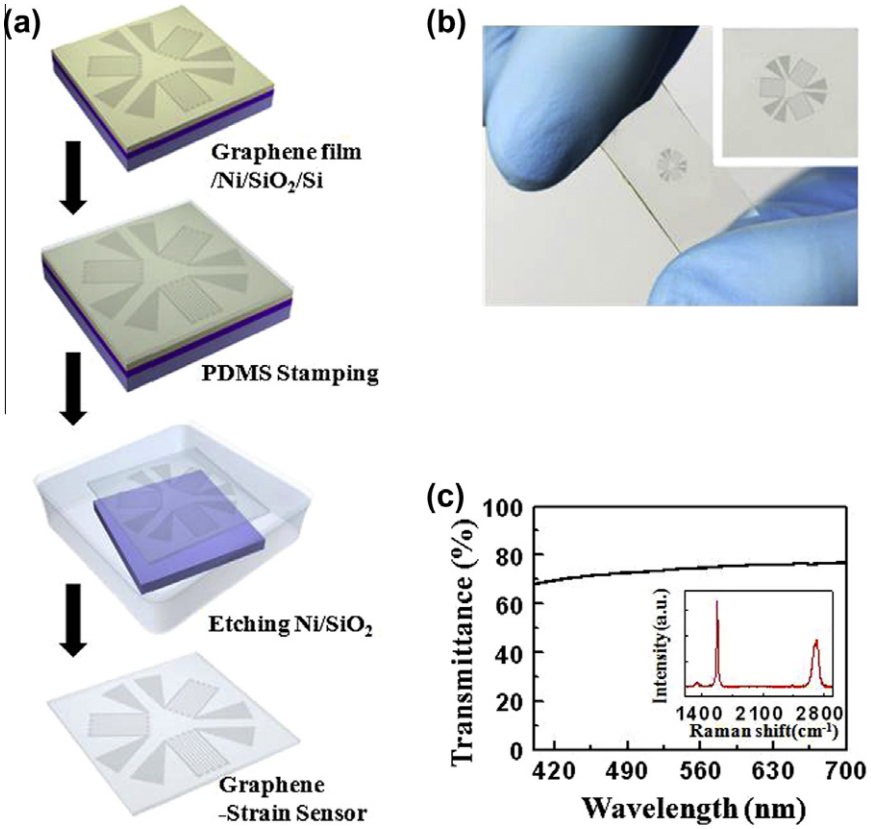

Fig. 1 – (a) Schematic representation of various steps in fabrication process. (b) Photograph of transparent graphene strain sensor. (c) Transmittance spectrum and inset shows the Raman spectrum of graphene film.

measurement was carried out at ambient conditions. When we dealt with the rosette type strain sensor, we measured the voltage signals of the three strain sensors simultaneously. The same motion controller used in previous stretching was utilized to make strain.

3. Results and discussion

The graphene-based strain sensor fabricated in this study shows good transparency (75–80%), as indicated by the transmission spectra shown in Fig. 1c. Since the individual graphene layer is supposed to reduce its transparency by ~2.3%, the number of layers grown in the present study can be approximated as 10 layers [23,24]. The inset of Fig. 1c shows the Raman spectra of as-grown graphene films. The observed strong peaks of the G and 2D bands at 1580 cm^{-1} and 2670 cm^{-1}, respectively, clearly revealed the successful synthesis of graphene films. The sheet resistance of graphene films was measured by the van der Pauw method with four probes, which was estimated to be ~500 Ω/sq in average.

3.1. *Piezoresistive effect*

Piezoresistive properties of the graphene strain sensors mounted on the PDMS thin film were investigated using a motorized tensile machine which was able to apply uniaxial tensile strain to a thin film material. Since the van der Waals force between graphene and PDMS provides a strong adhesion between them, graphene experiences the same strain level as the PDMS film. Fig. 2a shows a photograph of the measuring system used to investigate the piezoresistive properties of the graphene strain sensor under tensile strain. To remove the effect of wrinkles or ripples that can occur during the graphene synthesis and transfer processes, we define the point that graphene film is flat as an initial point. For the measurement of piezoresistive properties, the PDMS thin film with the graphene strain sensor was first machined in a form of strip with a length of 30.05 mm and a width of 50 μm on assumption that the all strip is straightened in a line. Then, both ends of the strip were fixed on sample holders with careful alignment between the tensile direction and the length direction of the strip, as shown in Fig. 2a. Afterwards, the graphene strain sensor on the PDMS film was stretched by the tensile machine step by step in a very small increment (~0.015%). Meanwhile, continuous voltage was applied through the graphene strain sensor to measure the change of electrical resistance during the tensile deformation of the sensor. In the unstrained position, the distance between two fixed points was measured as 21.95 mm (0%), and, for maximum strain (7.1%), it was measured as 23.48 mm. During the test, we continuously measured the electrical resistance as a function of the applied strain up to about 7.1%. As shown in Fig. 2b, the variation in normalized resistance increased continuously as the strain increases before the fracture of the graphene strain sensor. We found the existence of two different regions: (i) a nearly linear relationship between the resistance change and the strain when the applied strain is lower than 1.8%, and (ii) a nonlinear relationship when the strain is in the range between 1.8% and 7.1%. When the applied strain is larger than 7.1%, the strain sensor shows the abrupt increase in the resistance, which means that the device does not respond above this strain value due to mechanical fracture. In the first region lower than 1.8%, the gauge factor is about 2.4, which is comparable to that of the conventional metallic strain gauge. In contrast, in the second region, the gauge factor of the strain sensor over 1.8% ranges from 4 to 14.

We need to speculate the cause of these different phenomena. In the first region of low strain value, the change in the resistance of graphene with zero band gap could possibly increase because of the change in the carbon-carbon bond length during stretching, which exhibits the similar mechanism with conventional metallic materials. In this case, the gauge factor shows about 2.4. In contrast, in the second region of high strain value, the gauge factor shows higher value than one in the first region. When we consider various possible factors that affect the change of resistance such as effective mass, doping concentration, temperature, crystal imperfection and crystallographic axes, the imperfection of the material could be a strong candidate for explaining why the gauge factor becomes higher in the second region [25]. This phenomenon is also supported by the imperfect recovery of the electric current after 7% stretching as shown in Fig. 3b while the current perfectly recovers under 2% during a loading/unloading cycle as shown in Fig. 3a. That is, we swept voltage from 0 V to 0.05 V in both cases, under 2% strain and

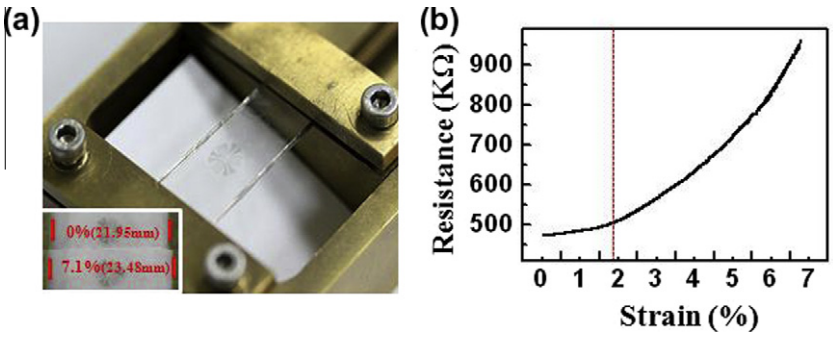

Fig. 2 – (a) Photograph of graphene strain sensor fixed in motion controller under stretching test. Inset shows the initial distance (~0%) and final distance (~7.1%) between two fixed points. (b) variation of resistance with respect to stretching up to ~7.1% for graphene strain sensor.

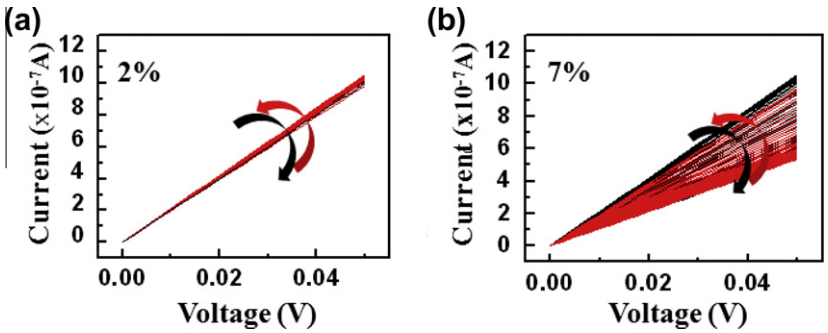

Fig. 3 – (a) Current–voltage (*I–V*) characteristics of graphene strain sensor under stretching up to ~2% (black and red lines indicate stretching and recovery respectively). (b) *I–V* characteristics of graphene strain sensor under stretching up to ~7% (black and red lines indicate stretching and recovery, respectively). (For interpretation of the references to color in this figure legend, the reader is referred to the web version of this article.)

7% strain. The current level perfectly recovered only for the case of 2%. This means that this graphene films on PDMS is useful as a strain sensor under strain of 2% in this particular case.

3.2. *Rosette type strain sensor*

A single strain sensor based on graphene has a merit of transparency, but is just capable of detecting the strain or deformation in a single direction that is pre-defined by attaching the strain sensor on a substrate. It limits the uses of the transparent strain sensors in real-life applications, such as biomedical applications where we need to make a conformal contact with the human body and need to monitor the complicated motions or deformations of body parts in addition to the optical observation through the strain sensor. For characterization of the complicated deformation state on a surface, it is necessary to measure three different components of strain tensor, ε_x, ε_y and γ_{xy} with respect to a given coordinate system. Therefore, to further explore the possible application of graphene-based strain sensors in real life, we arranged the three identical strain sensors in a form of rosette, oriented at 120° to each other in the equilateral triangular configuration. This kind of arrangement of three equally spaced identical coplanar strain sensors making a fixed angle of 60° with each other is called by the planar 60-delta rosette gauge system (Fig. 4a). The strain sensors in the rosette gauge arrangement are named as *a*, *b*, and *c*, and their corresponding strain values can be denoted as ε_a, ε_b, and ε_c. Using the predefined directions and the measured strain magnitudes of three strain gauges, it is possible to determine the full state of strain on a surface (three independent strain components) at the gauge location. This can be illustrated using the "strain transformation method," known as Mohr's circle, which can be represented graphically for a surface state of strain as shown in Fig. 4b [26]. The normal strain at any angle θ from the major principal axis can be expressed as:

$$\varepsilon_\theta = \frac{\varepsilon_x + \varepsilon_y}{2} + \frac{\varepsilon_x - \varepsilon_y}{2}\cos 2\theta \tag{1}$$

When the principal strains are oriented at an angle θ with respect to the rosette gauge *a*-axis, then the strain in each rosette gauge, ε_a, ε_b, and ε_c, can be represented in terms of principal strains ε_x and ε_y with the corresponding rotation angles θ, $\theta + 60°$, and $\theta + 120°$, using the following strain transformation equations:

$$\varepsilon_a = \frac{\varepsilon_x + \varepsilon_y}{2} + \frac{\varepsilon_x - \varepsilon_y}{2}\cos 2\theta \tag{2a}$$

$$\varepsilon_b = \frac{\varepsilon_x + \varepsilon_y}{2} + \frac{\varepsilon_x - \varepsilon_y}{2}\cos 2(\theta + 60) \tag{2b}$$

$$\varepsilon_c = \frac{\varepsilon_x + \varepsilon_y}{2} + \frac{\varepsilon_x - \varepsilon_y}{2}\cos 2(\theta + 120) \tag{2c}$$

The right-hand side variables in Eq. (2) are unknown; whereas, the strains in each rosette gauge, ε_a, ε_b, and ε_c, can be experimentally measured directly from the rosette gauge arrangement. Therefore, the unknown variables, principal strains ε_x and ε_y, and their orientation θ can be expressed in terms of known quantities ε_a, ε_b, and ε_c as follows:

$$\varepsilon_{x,y} = \frac{\varepsilon_a + \varepsilon_b + \varepsilon_c}{3} \pm \frac{\sqrt{2}}{3}\sqrt{(\varepsilon_a - \varepsilon_b)^2 + (\varepsilon_b - \varepsilon_c)^2 + (\varepsilon_c - \varepsilon_b)^2} \tag{3}$$

$$\theta = \frac{1}{2}\tan^{-1}\left(\frac{\sqrt{3}(\varepsilon_b - \varepsilon_c)}{2\varepsilon_a - \varepsilon_b - \varepsilon_c}\right) \tag{4}$$

The '±' alternatives in Eq. (3) yield the algebraically maximum (ε_x) and minimum (ε_y) principal strain, respectively, in Mohr's circle.

The strain sensing properties of the fabricated rosette gauge under stretching were investigated by the same measurement system as that described earlier in Fig. 2a, except that the resistance change of all three strain sensors was measured simultaneously. Fig. 4c shows the simultaneous measurement of normalized resistance as a function of applied strain up to 1.5% for all the three gauges in the rosette arrangement. Stretching was carried out along *a*-axis, such that the '*a*' gauge and the other two gauges, '*b*' and '*c*', are positioned at the same distance and are oriented at the same angle with respect to the '*a*' gauge. The resistances measured from the three gauges increase continuously as the increase of the strain, and the change in the normalized resistance from the '*a*' gauge is much larger than that from the '*b*' and '*c*' gauges. The behavior of resistance change as a function of strain up to 1.5% for all these three gauges ('*a*', '*b*', and '*c*') in rosette arrangement matches well with that of our single graphene-based strain sensor, which is discussed in Fig. 2b.

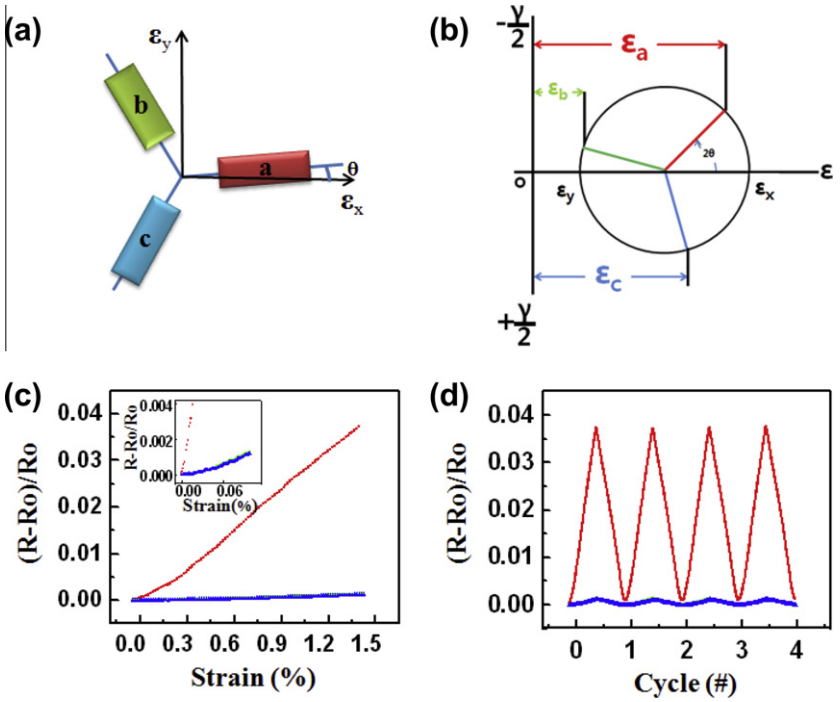

Fig. 4 – (a) Schematic representation of graphene strain sensor in Rosette manner indicating the direction of principle axis. (b) Mohr's circle diagram used in strain analysis. (c) Variation of normalized resistance with respect to stretching up to 1.5% (inset shows for low strain values ~0.08%) and (d) cyclic test for graphene based Rosette strain gauge; the red, the green, and blue indicate the data of the gauge a, the gauge b, and gauge c, respectively. (For interpretation of the references to color in this figure legend, the reader is referred to the web version of this article.)

This indicates that each graphene strain sensor in a rosette gauge does not degrade with respect to applied strain for the strain value less than 1.5%. Strain values ε_a, ε_b, and ε_c corresponding to three strain sensors, '*a*', '*b*', and '*c*', from the resistance-change data are calculated as 1.5%, 0.052%, and 0.048%, when the external strain of about 1.5% is applied to the sample by the motorized tensile machine. As we already discussed, when we know the values of three independent strains from three gauges arranged in the rosette, the principal strains and their orientation with respect to the rosette axis can be estimated. Principal strains ε_x and ε_y and their angle of orientation are calculated by inserting the three strain values of the three gauges to Eqs. (3) and (4), and are found to be 1.5%, −0.42%, and 0.1°. The calculated value 1.5% of the maximum principal strain (ε_x) matches with the externally applied strain value by the tensile machine, and this indicates the good accuracy and sensing capability of the proposed graphene-based transparent rosette gauge. In addition, when considering that the Poisson's ratio of the PDMS is ~0.3–0.4, the calculated value for ε_y is also reasonable [27]. The stability of the fabricated rosette gauge was tested by performing loading and unloading tests several times. Fig. 4d shows the simultaneous cyclic measurement of three identical strain sensors, '*a*', '*b*', and '*c*', arranged in the rosette manner. The change in normalized resistance characteristics repeated perfectly several times as the gradual increase and subsequent decrease of the applied strain, and this verified that the fabricated graphene rosette gauge showed a very stable capability of sensing strain under the repeated measurements.

3.3. *Glove sensor*

For further realization of the potential utilization of the proposed graphene rosette gauge for wearable electronics, we fabricated three identical strain sensors in a rosette manner on a wearable and stretchable glove in such a way that when wearing the glove, the rosette gauge was located on the back side of the finger joint as shown in the inset of Fig. 5a. Here, we used epoxy (<1 μm) as an adhesive to make the rubber glove and strain sensor tightly bonded to each other. This demonstration reveals the sensitivity of the rosette gauge against the finger motion: as we start to bend the finger, the strain created by the bending motion of the finger is adopted by the first glove layer and then, propagated to the rosette gauge. The rosette gauge immediately responded to the bending of the finger, and its signal amplitude depends on the value of the strain created by the finger bending: as more the finger bends, more the signal amplitude increases. When the finger bends, the signal appears and when we straighten it, the signal disappears, as is shown in Fig. 5a for continuous bending and straightening of the finger. The strain value created by bending the finger is approximated as 1.3%, 1.2%, 1.4% and 1.6% respectively, based on the change in resistance and the strain sensor recovered perfectly after straightening the finger. Here, we aligned the strain sensor in the direction of strain. Therefore, the measured strain can be regarded as principal strain on the surface. Moreover, the strain sensors perform perfectly after much repeated bending and straightening of the finger, thus showing good durability. In addition

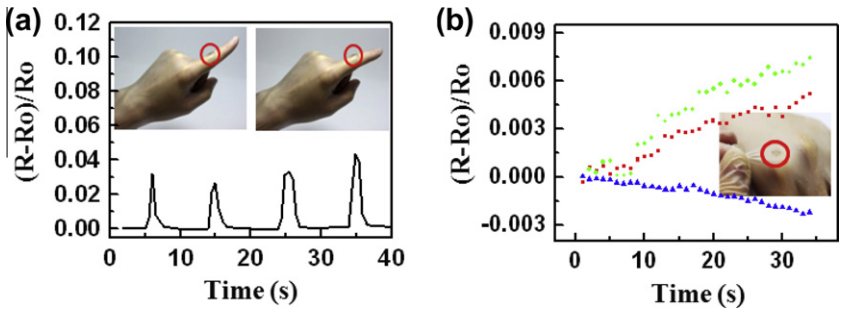

Fig. 5 – (a) Repeatedly increase and decrease in normalized resistance of graphene strain sensor mounted on finger of wearable glove (inset) with respect to monitoring the finger motion up and down. (b) Variation in normalized resistance with respect to time during stretching of graphene based Rosette gauge mounted on wearable glove (inset); the red, the green, and blue indicate the data of the gauge a, the gauge b, and gauge c, respectively. (For interpretation of the references to color in this figure legend, the reader is referred to the web version of this article.)

to the bending test, a stretching test was also carried out to estimate the principal strains and their orientations. To demonstrate the stretching test, we mounted the rosette gauge on a wearable glove and slowly and gently stretched the thin material of the glove by hand, as shown in the inset of Fig. 5b, and measured the resistance change under stretching. Fig. 5b shows the simultaneous resistance change measurement of three strain sensors mounted on a wearable glove in a rosette manner. Under such non-coplanar stretching, the amount of strain adopted by three independent sensors is quite different. We determined the strain values ε_a, ε_b, and ε_c, corresponding to three strain sensors, '*a*', '*b*', and '*c*', from their resistance-change data and the gauge factor of graphene, and the strain values were 0.52%, 0.74%, and −0.22%, respectively. After substituting the strain values of ε_a, ε_b, and ε_c in Eqs. (3) and (4), the principal strains ε_x and ε_y and their orientation were calculated as 0.92%, −0.24%, and 36.2°, respectively. Thus, graphene based strain sensor assembled with glove exhibits the capability to defect simultaneously both force and direction of external strain.

4. Summary

We fabricated a transparent and stretchable strain sensor based on CVD-grown graphene and investigated its piezoresistive properties under stretching. Results show that a non-monotonic resistance change against tensile strain up to 7.1%. This non-linear behavior of the proposed graphene strain sensor is attributed to the creation of defects, disorders, and micro-cracks. We also successfully demonstrated the transparent rosette gauge on a stretchable and wearable hand glove to overcome the limits of single strain sensors and for simultaneous detection of the magnitude and direction of the principal strains during bending motion of a finger.

Acknowledgements

This work was supported by the National Research Foundation of Korea (NRF) (2009-0083540, 2012-006049), and a Grant-in-Aid for Industrial Source Technology Development Programs from the Korea Ministry of Knowledge Economy (No. 10033309).

REFERENCES

[1] He R, Yang P. Giant piezoresistance effect in silicon nanowires. Nat Nanotechnol 2006;1(1):42–6.
[2] Laukhina E, Pfattner R, Ferreras LR, Galli S, Mas-Torrent M, Masciocchi N, et al. Ultrasensitive piezoresistive all-organic flexible thin films. Adv Mater 2010;22(9):977–81.
[3] Zhang J, Liu J, Zhuang R, Mäder E, Heinrich G, Gao S. Single MWNT-glass fiber as strain sensor and switch. Adv Mater 2011;23(30):3392–7.
[4] Lipomi DJ, Vosgueritchian M, Tee BCK, Hellstrom SL, Lee JA, Fox CH, et al. Skin-like pressure and strain sensors based on transparent elastic films of carbon nanotubes. Nat Nanotechnol 2011;6(12):788–92.
[5] Lee C, Wei X, Kysar JW, Hone J. Measurement of the elastic properties and intrinsic strength of monolayer graphene. Science 2008;321(5887):385–8.
[6] Kim BJ, Jang H, Lee S-K, Hong BH, Ahn J-H, Cho JH. High-performance flexible graphene field effect transistors with ion gel gate dielectrics. Nano Lett 2010;10(9):3464–6.
[7] Liu Z, Liu Q, Huang Y, Ma Y, Yin S, Zhang X, et al. Organic photovoltaic devices based on a novel acceptor material: graphene. Adv Mater 2008;20(20):3924–30.
[8] Han T-H, Lee Y, Choi M-R, Woo S-H, Bae S-H, Hong BH, et al. Extremely efficient flexible organic light-emitting diodes with modified graphene anode. Nat Photon 2012;6(2):105–10.
[9] Wang Y, Tong SW, Xu XF, Özyilmaz B, Loh KP. Interface engineering of layer-by-layer stacked graphene anodes for high-performance organic solar cells. Adv Mater 2011;23(13):1514–8.
[10] Kim R-H, Bae M-H, Kim DG, Cheng H, Kim BH, Kim D-H, et al. Transparent graphene interconnects for arrays of microscale inorganic light emitting diodes on rubber substrates. Nano Lett 2011;11(9):3881–6.
[11] Lee Y, Bae S, Jang H, Jang S, Zhu S-E, Sim SH, et al. Wafer-scale synthesis and transfer of graphene films. Nano Lett 2010;10(2):490–3.
[12] Fu X-W, Liao Z-M, Zhou J-X, Zhou Y-B, Wu H-C, Zhang R, et al. Strain dependent resistance in chemical vapor deposition grown graphene. Appl Phys Lett 2011;99(21):213107.
[13] Huang M, Pascal TA, Kim H, Goddard WA, Greer JR. Electronic–mechanical coupling in graphene from in situ nanoindentation experiments and multiscale atomistic simulations. Nano Lett 2011;11(3):1241–6.

[14] Wang Y, Yang R, Shi Z, Zhang L, Shi D, Wang E, et al. Super-elastic graphene ripples for flexible strain sensors. ACS Nano 2011;5(5):3645–50.
[15] Frank O, Tsoukleri G, Riaz I, Papagelis K, Parthenios J, Ferrari AC, et al. Development of a universal stress sensor for graphene and carbon fibres. Nat Commun 2011;2:255.
[16] Yamada T, Hayamizu Y, Yamamoto Y, Yomogida Y, Izadi-Najafabadi A, Futaba DN, et al. A stretchable carbon nanotube strain sensor for human-motion detection. Nat Nanotechnol 2011;6(5):296–301.
[17] Loh K, Hou T-C, Lynch J, Kotov N. Carbon nanotube sensing skins for spatial strain and impact damage identification. J Nondestr Eval 2009;28(1):9–25.
[18] Cao J, Wang Q, Dai H. Electromechanical properties of metallic, quasimetallic, and semiconducting carbon nanotubes under stretching. Phys Rev Lett 2003;90(15):157601.
[19] Prasad D, Zhiling L, Satish N, Barrera EV. Nanotube film based on single-wall carbon nanotubes for strain sensing. Nanotechnology 2004;15(3):379.
[20] Kang JH, Park C, Scholl JA, Brazin AH, Holloway NM, High JW, et al. Piezoresistive characteristics of single wall carbon nanotube/polyimide nanocomposites. J Pol Sci Part B: Pol Phys 2009;47(10):994–1003.
[21] Rogers JA, Someya T, Huang Y. Materials mechanics for stretchable electronics. Science 2010;327(5973):1603–7.
[22] Kim KS, Zhao Y, Jang H, Lee SY, Kim JM, Kim KS, et al. Large-scale pattern growth of graphene films for stretchable transparent electrodes. Nature 2009;457(7230):706–10.
[23] Bae S, Kim H, Lee Y, Xu X, Park J-S, Zheng Y, et al. Roll-to-roll production of 30-inch graphene films for transparent electrodes. Nat Nanotechnol 2010;5(8):574–8.
[24] Nair RR, Blake P, Grigorenko AN, Novoselov KS, Booth TJ, Stauber T, et al. Fine structure constant defines visual transparency of graphene. Science 2008;320(5881):1308.
[25] Kittel C. Introduction to solid state physics/Charles Kittel. New York: Wiley; 1976. p. 89–218.
[26] Mase Geprge E. Schaum's outline of continuum mechanics. McGraw-Hill; 1969. p. 91–2.
[27] Jiang H, Khang D-Y, Song J, Sun Y, Huang Y, Rogers JA. Finite deformation mechanics in buckled thin films on compliant supports. Proc Natl Acad Sci 2007;104(40):15607–12.